Multi-wavelength Analysis of $18\,\mu$m-selected Galaxies in the AKARI/IRC monitor field towards the North Ecliptic Pole

Toshinobu TAKAGI,[1] * Hideo MATSUHARA,[1] Takehiko WADA,[1] Shinki OYABU,[1]
Koji IMAI,[1] Chris P. PEARSON,[1,2] Hitoshi HANAMI,[3] Takashi ONAKA,[4]
Naofumi FUJISHIRO,[1] Daisuke ISHIHARA,[4] Yoshifusa ITA, [1] Hirokazu KATAZA,[1]
Woojung KIM,[1] Toshio MATSUMOTO,[1] Hiroshi MURAKAMI,[1] Youichi OHYAMA,[1]
Itsuki SAKON,[4] Toshihiko TANABÉ,[5] Kazunori UEMIZU,[1] Munetaka UENO,[6]
Hidenori WATARAI,[7] Fumihiko USUI,[1] Hyung Mok LEE,[8] Myungshin IM,[8]
Stephen SERJEANT,[9] Richard S. SAVAGE,[10]
Tsutomu TANGE,[1] and Takao NAKAGAWA[1]

[1] *Institute of Space and Astronautical Science, Japan Aerospace Exploration Agency,*
Sagamihara, Kanagawa 229-8510
[2] *ISO Data Centre, ESA, Villafranca del Castillo, Madrid, Spain.*
[3] *Physics Section, Faculty of Humanities and Social Sciences,*
Iwate University, Morioka, 020-8550
[4] *Department of Astronomy, School of Science, University of Tokyo,*
Bunkyo-ku, Tokyo 113-0033
[5] *Institute of Astronomy, University of Tokyo, Mitaka,Tokyo 181-0015*
[6] *Department of Earth Science and Astronomy, Graduate School of Arts and Sciences,*
The University of Tokyo, Meguro-ku,Tokyo 153-8902
[7] *ALOS Project, Japan Aerospace Exploration Agency, Tsukuba, Ibaraki 305-8505*
[8] *Department of Physics & Astronomy, FPRD, Seoul National University,*
Shillim-Dong, Kwanak-Gu, Seoul 151-742, Korea
[9] *Astrophysics Group, Department of Physics,*
The Open University, Milton Keynes, MK7 6AA, UK
[10] *Astronomy Centre, University of Sussex, Falmer, Brighton BN1 9QJ, UK*

Abstract

We present an initial analysis of AKARI $18\,\mu$m-selected galaxies using all 9 photometric bands at 2 – $24\,\mu$m available in the InfraRed Camera (IRC), in order to demonstrate new capabilities of AKARI cosmological surveys with this unprecedented wavelength coverage at mid-infrared bands. We detected 72 sources at $18\,\mu$m in an area of 50.2 arcmin^2 in the AKARI/IRC monitor field towards the North Ecliptic Pole (NEP). From this sample, 25 galaxies with probable redshifts $z \gtrsim 0.5$ are selected with a single colour cut ($N2 - N3 > 0.1$) for a detailed SED analysis with ground-based $BVRi'z'JK$ data. Using an SED radiative transfer model of starbursts covering the wavelength range UV – submm, we derive photometric redshifts from the optical-MIR SEDs of $18\,\mu$m-selected galaxies. From the best-fit SED models, we show that the IRC all-band photometry is capable of tracing the steep rise in flux at the blue side of the PAH $6.2\,\mu$m emission feature. This indicates that the IRC all-band photometry is useful to constrain the redshift of infrared galaxies, specifically for dusty galaxies with a less prominent $4000\,\text{Å}$ break. Also, we find that the flux dip between the PAH 7.7 and $11.2\,\mu$m emission feature is recognizable in the observed SEDs of galaxies at $z \sim 1$. By using such a colour anomaly due to the PAH and silicate absorption features, unique samples of ULIRGs at $z \sim 1$, 'silicate-break' galaxies, can be constructed from large cosmological surveys of AKARI towards the NEP, i.e. the NEP-Deep and NEP-Wide survey. For AGN candidates selected with an IRC colour-colour diagram ($N2 - N3$ vs. $N3 - S7$), we find excess emission in more than two MIR bands, compared to the best-fit starburst SED model, which suggests the presence of hot dust around the central black hole. This pilot study suggests the possibility of detecting many interesting galaxy properties in the NEP-Deep and Wide surveys, such as a systematic difference in SEDs between high- and low-z ULIRGs, and a large variation of the PAH inter-band strength ratio in galaxies at high redshifts.

Key words: infrared: galaxies — galaxies: starburst — galaxies: active — galaxies : evolution

1.   Introduction

The universe is a much more luminous place than seen in the optical, so it has been revealed since the launch of the first infrared astronomical satellite, IRAS (Neugebauer et al., 1984). Subsequent infrared space missions, i.e. ISO (Kessler et al., 1996) and Spitzer (Werner et al., 2004) have led to enormous advances in our knowledge on star-formation activity, specifically in the distant universe (e.g. Genzel & Cesarsky, 2000; Franceschini et al., 2006, and references therein). The last mission, AKARI was launched on 22nd February 2006 JST (Murakami et al., 2007) and is functioning very well in orbit at the time of writing.

The deepest extragalactic surveys for infrared luminous galaxies have been carried out at $15\,\mu$m with ISO and $24\,\mu$m with Spitzer, due to the fact that the confusion of point sources and of background cirrus emission is more serious in longer wavelengths. A key result from ISO surveys may be summarised in the differential number counts at $15\,\mu$m (see e.g. Figure 14 in Genzel & Cesarsky, 2000), which have a characteristic bump at around $300\,\mu$Jy. With these number counts, pure density evolution models are clearly rejected, and strong luminosity evolution with $\sim (1+z)^4$ is suggested at $0 < z < 1$ (Xu, 2000; Pearson, 2001; Franceschini et al., 2001; Chary & Elbaz, 2001). Recently, this strong luminosity evolution at $0 < z < 1$ has been confirmed by Spitzer with much greater statistical significance (Pérez-González et al., 2005; Babbedge et al., 2006; Caputi et al., 2007).

Multi-wavelength surveys at *both* 15 and $24\,\mu$m are not just redundant observations, but reveal the problems in our understanding of distant infrared galaxies. Although the differential number counts at $24\,\mu$m are found to be similar in shape to the $15\,\mu$m counts, it is not straightforward to explain the $24\,\mu$m counts with the phenomenological models of galaxy counts constrained to fit the multi-wavelength counts prior to the Spitzer results. The peak in the $24\,\mu$m differential counts is found at $200 - 300\,\mu$Jy (in $dN/dS \times S^{2.5}$) which is fainter than expected from models of galaxy counts. The resolution of this problem has not yet been achieved (see however Lagache et al., 2004; Chary et al., 2004; Pearson, 2005). Since at 15 and $24\,\mu$m we observe the PAH emission features of galaxies at $z = 1 - 3$, we need SED templates with realistic PAH emission features as a function of luminosity for galaxies at $z > 1$. Unfortunately, such SED templates are not yet available.

With the InfraRed Spectrograph (IRS) onboard Spitzer, MIR features of high-z galaxies, such as the PAH emission feature and silicate absorption feature, become accessible (Houck et al., 2005; Lutz et al., 2005; Yan et al., 2005; Huang et al., 2006; Weedman et al., 2006; Menéndez-Delmestre et al., 2007; Teplitz et al., 2007), although the observed samples are still very limited. The highest redshift PAH detection has been reported in an infrared-luminous Lyman break galaxy at $z = 3.01$ (Huang et al.,

2006), which is likely to be a hyperluminous infrared galaxy. Currently, the prime high-z targets for IRS seem to be submm galaxies (Lutz et al., 2005; Menéndez-Delmestre et al., 2007; Pope et al., 2006). It is rather surprising that PAH emission features are detected in most submm galaxies, given that they are typically hyperluminous ($L_{IR} > 10^{13}L_\odot$) galaxies which are in the local universe generally AGN-dominated galaxies. There is already a hint that the MIR properties of high-z galaxies are systematically different to those in the local universe. More systematic studies on this issue are clearly needed.

With Spitzer surveys, the majority of Hyper- and Ultra-Luminous InfraRed Galaxy (Hy/ULIRGs)[1] targets at high redshifts may be derived from the $24\,\mu$m source catalogues. This may result in incomplete samples of ULIRGs specifically at $z \sim 1.5$, at which ULIRGs with strong silicate absorption become very faint in the $24\,\mu$m band (Takagi & Pearson, 2005; Armus et al., 2007). Caputi et al. (2006) obtained a bimodal redshift distribution of $24\,\mu$m sources as a result of the deficit of galaxies at $z \sim 1.5$ (see also Franceschini et al., 2006). More comprehensive wavelength coverage at MIR bands should be useful to produce complete samples of ULIRGs at $1 < z < 2$. We point out below that the AKARI multi-wavelength surveys are best suited for this purpose, thanks to their superb wavelength coverage in the NIR – MIR.

The most unique scientific programme of AKARI is the all-sky survey, the first major update of IRAS. Besides this, another uniqueness of AKARI can be found in surveys of selected areas with unprecedented wavelength coverage in the NIR – MIR, with 9 photometric bands from 2 to $24\,\mu$m using the InfraRed Camera (IRC; Onaka et al., 2007). With the IRC, two main extragalactic surveys have been designed and conducted around the North Ecliptic Pole (NEP), a deep $\sim 0.5\,\mathrm{deg}^2$ survey (the NEP-Deep survey) and a shallow $6.2\,\mathrm{deg}^2$ survey (the NEP-Wide survey). See Matsuhara et al. (2006) for details on the survey design of the NEP-Deep and NEP-Wide surveys.

With this comprehensive wavelength coverage, one clear benefit for extragalactic MIR surveys is that a more reliable selection for high-z ULIRGs becomes possible, as noted above. In a flux limited sample with Spitzer MIPS $24\,\mu$m, it is likely that some fraction of ULIRGs at $z \sim 1.5$ are missed, owing to redshifted silicate absorption features. With IRC, such ULIRGs would be detected at 15 and/or $18\,\mu$m. These ULIRGs may be called $24\,\mu$m dropouts or 'silicate-break' galaxies (Takagi & Pearson, 2005). This capability would be very useful to make a complete sample of MIR-bright ULIRGs for follow-up observations with MIR spectroscopy. Furthermore, the resulting well-sampled SEDs of MIR-selected galaxies allow us to study the nature of distant infrared galaxies in detail with the help of SED models, including the photometric estimation of redshifts from MIR features.

As a pilot study for a full analysis of the NEP survey, here we report the first insight on AKARI $18\,\mu$m-selected

*   E-mail: takagi@ir.isas.jaxa.jp

---

[1]   [Hy,U]LIRGs defined with $\log L_{IR}/L_\odot = [> 13,\ 12 - 13]$, where L_{IR} is the luminosity in the wavelength rage from 8 to $1000\,\mu$m.

distant infrared galaxies seen by all 9 photometric bands available in the IRC. Lee et al. (2007) provide similar study for an AKARI 11 μm-selected sample with 6 photometric bands between 2 and 11 μm. Matsuhara et al. (2007) report the optical properties of an AKARI 15 μm-selected sample taken from Wada et al. (2007) in which results of a deep 15 μm survey during the performance verification phase are presented. In section 2, we describe our data and reduction method using the IRC monitor observations. For detailed analysis of 18 μm-selected galaxies, we focus on galaxies likely to lie at $z \gtrsim 0.5$, i.e. the main targets of interests in the NEP survey. Then, we analyse these galaxies with the SED radiative transfer model of starbursts from Takagi et al. (2003b,a). In sections 3 and 4, we give our selection method for galaxies at $z \gtrsim 0.5$ and the SED fitting method, respectively. Results are described in section 5. In section 6, we attempt to identify silicate-break galaxies in our sample. We summarise our study in section 7. Throughout this paper, we adopt the cosmology of $\Omega_m = 0.3$, $\Omega_\Lambda = 0.7$ and $H_0 = 70 \, \mathrm{km \, sec^{-1} Mpc^{-1}}$. All magnitudes are given in the AB system, unless otherwise explicitly noted.

2.   Observations and data reduction

2.1.   Data from AKARI

We have used the IRC monitor observations near the NEP with a field centre of $\alpha = 17^{\mathrm{h}}55^{\mathrm{m}}24^{\mathrm{s}}$, $\delta = +66°37'32''$ (J2000), covering one field of view ($\sim 10' \times 10'$) by all 9 IRC photometric bands, i.e. $N2$, $N3$, $N4$, $S7$, $S9W$, $S11$, $L15$, $L18W$ and $L24$. This field is regularly monitored with the IRC, in order to check the stability of the detectors. Wada et al. (2007) report a deep survey of this field at 3 and 7 μm, which was conducted during the performance verification phase. The observations were done with the Astronomical Observation Template (AOT) three filter mode, IRC03 (see Onaka et al. 2007 for details). During one pointed observation, three IRC channels, NIR, MIR-S and MIR-L can operate simultaneously, covering different wavelength ranges. The NIR and MIR-S channels share the same field of view, while the MIR-L channel observes a region $\sim 20'$ away from the field centre of NIR/MIR-S. In this paper, we use the data from 17 NIR/MIR-S pointed observations conducted between 19th June and 4th December 2006, and 5 MIR-L pointed observations between 28th June and 30th July 2006. We summarise the observation parameters in Table 1.

2.2.   Reduction

We reduced the data with the IRAF-based IRC pipeline software[2] (Onaka et al. 2007), in order to remove and correct the basic instrumental effects: dark subtraction, linearity correction, distortion correction and flat fielding. With the AOT IRC03, there is a sufficient number of frames per band (6 − 9 frames) during one pointed observation to coadd the MIR-S data and also the MIR-L

data. We coadded the MIR-S frames from each pointed observation using the IRC pipeline in which sky positions of detected point sources are matched to calculate the relative astrometric shift between the frames. We did this after subtracting the sky background. For MIR-L, it was found that the sky background is too high and sources are too faint to match the positions of point sources. We used an optional command of the IRC pipeline (`coaddLusingS`) to coadd the MIR-L images, in which the relative astrometric shifts of the MIR-L images are derived from those of the MIR-S images by adopting the calibration of the relative offset between the MIR-L and the MIR-S channels. Thus we obtained coadded images of MIR-S and MIR-L for each pointed observation.

In order to coadd images from different pointed observations, we used the publicly available software SWarp[3], after putting the world coordinate system (WCS) on each image. We put the WCS for the MIR-S images using the IRC pipeline command `putwcs` in which 2MASS sources are identified and the astrometric solution is derived from them. For MIR-L, we manually identified three bright sources detected both in the MIR-L images and in the final $S11$ image, then determined the WCS for the MIR-L images. We used a median coaddition to produce the final images.

For the NIR channel, we put the WCS into each individual frame using `putwcs`. This was successful for all of the NIR frames, although there is a large number of cosmic ray hits in each frame. Again, SWarp was used to obtain the final images with median coaddition.

2.3.   Source detection and photometry on the IRC images

Source detection was performed in a circular area of the final $L18W$ image which has a radius of 4 arcmin covering the deepest region. We used SExtractor (Bertin & Arnouts, 1996) in which two or more connected $> 3\sigma$ pixels are identified as a source. This threshold results in the detection of sources with the signal-to-noise ratio of $\gtrsim 4.5$. This parameter setting for SExtractor is a result of our optimization to detect reliable point sources and avoid fainter extended sources which are likely to be residuals of the background subtraction. We have detected 72 sources in the area of 50.2 arcmin^2.

Since all of the 18 μm sources are found to have a counterpart at other IRC bands, the reliability of the detected sources is very high. We applied the same source detection method for the negative $L18W$ image, and detected only 5 sources. From an inspection of the negative image, it is obvious that they are not point sources like those detected in the positive image, but rather a result of the negative extended pattern caused by the residuals of the sky subtraction. We also used the negative $L18W$ image to estimate the typical photometric error. On the negative $L18W$ image, we performed aperture photometry at random source-free positions (determined in the positive image) using the same procedure as with detected sources (see below). The distribution of flux measured

at random positions has the standard deviation of $25\,\mu$Jy, which represents a typical photometric error. We note that the faintest source in our catalogue has the flux of $129\pm27\,\mu$Jy.

In the other IRC bands, we identified the counterparts of the detected $18\,\mu$m sources by using the sky coordinates from SExtractor. First, we determined the centroid of the counterparts (with `gcntrd.pro` in the IDL astronomy user's library[4]) using the sky coordinates of the $18\,\mu$m sources as the initial approximation of the centroid. If the newly-determined centroid is shifted from the original position by $>3''$, we rejected such a source as the counterpart of the $18\,\mu$m source. We found that this method results in a higher success rate of finding the counterparts of $18\,\mu$m sources than the comparison of source catalogs from each IRC band with a certain search radius. We visually inspected the result of the cross-identifications in postage stamp images (shown in Figures 3 & 4 for the colour selected sample, see below), and verified the correctness of the cross-identifications.

We performed aperture photometry at the centroid positions of the $18\,\mu$m sources and their counterparts in our IRC images. We used aperture radii of 2 and 3 pixels for the NIR and the MIR-S/L images, respectively. Note that in the flux calibration of the IRC images with standard stars, aperture radii of 10 and 7.5 pixels were used for the NIR and MIR-S/L channels, respectively. The aperture corrections used to estimate the total fluxes have been obtained from the empirical PSF derived from bright sources. For the NIR channel, we used bright sources in our images. For the MIR-S and the MIR-L channels, IRAS sources have been used which are detected in the observations for the NEP-Wide survey.

We found that the measured fluxes in the coadded NIR and MIR-S images are systematically lower than those before coaddition. This is because we coadded the images, which have elongated PSFs, with various position angles using a simple median. Using the empirical PSFs, we generated 'coadded' PSFs adopting the same position angle of the actual observations. The correction factors for this effect were estimated from aperture photometry of PSFs before and after coaddition. The correction factors are found to be 5% for $N2$, 7% for $N3$ and $N4$, and 3 % for the MIR-S channel.

We have not applied colour corrections for the IRC photometry at this initial stage of data reduction activity. The total error on the IRC photometry is estimated about $10 - 20$ %.

2.4. Optical identification

The IRC monitor field lies inside the NEP-Deep survey area and is covered by the deep $BVRi'z'$ optical observations with Subaru/S-cam, reaching $B = 28.4$ to $z' = 26.2$ AB mag in 5σ (Wada et al. 2007, in prep). This field is also covered by KPNO2.1m/FLAMINGOS at J- and Ks-band with a depth of $J = 21.6$ and $K_s = 19.9$ (3σ) in Vega magnitudes (Field-NE in Imai et al., 2007).

Since the astrometric accuracy is better for shorter wavelengths in the IRC bands, we adopted the positions from the NIR channel to find the optical counterparts of the $18\,\mu$m sources. We used the catalogue of FLAMINGOS K_s-band sources with optical Subaru/S-cam identifications taken from Imai et al. (2007). We identified the nearest K_s-band source as the $18\,\mu$m source counterpart. The resulting identifications were all visually inspected. If the angular separation is larger than $3''$, we reject the counterpart without visual inspection. We found no K_s-band counterparts for three $18\,\mu$m sources, for which we searched for the nearest optical counterpart from the Subaru/S-cam catalogue from Wada et al. (2007, in prep). A typical angular separation between the IRC positions and the optical positions is found to be $0.6'' \pm 0.2''$.

3. Sample selection

We have detected 72 sources in total at $18\,\mu$m, which include stars and galaxies at various redshifts. Since the main targets of this study and of the NEP surveys are star-forming galaxies at moderate – high redshifts, we adopt a simple colour cut to reduce the contamination from low redshift ($z \lesssim 0.5$) galaxies and stars.

We did this selection by following Huang et al. (2004) in which $z > 0.6$ galaxies are selected using only the $K - [3.6\mu m]$ colour by utilizing the $1.6\,\mu$m bump. Similar colour selection is possible with the IRC bands, i.e. $N2 - N3$ and/or $N2 - N4$. In order to confirm the effectiveness of this single colour selection, we derived photometric redshifts of the $18\,\mu$m sources from the ground-based optical-NIR SEDs by using $hyperz$ (Bolzonella et al., 2000). We adopted the SED templates of Bruzual & Charlot (2003) distributed with the source code of $hyperz$. In Figure 1, we plot the derived photometric redshifts against $N2 - N3$ and $N2 - N4$ colours. There is a clear correlation between z_{hyperz} and the AKARI NIR colours. This correlation confirms that a rough selection of $z \gtrsim 0.5$ galaxies is possible using only the single AKARI NIR colour. We prefer single colour cuts to photometric redshifts for the selection of galaxies at $z \gtrsim 0.5$, due to their simplicity and availability over the entire field of the NEP survey.

In the following we focus on the 25 galaxies satisfying the colour cut $N2 - N3 > 0.1$ which are likely to lie at $z \gtrsim 0.5$. In this sample, we include ID65 which nevertheless has $N2 - N3 < 0.1$ with large errors, since its $N2 - N4$ is similar to those of the other $N2 - N3$ selected galaxies and also its overall SED indicates that N2 flux is likely to be overestimated. As shown in Figure 1, a similar selection of galaxies is possible with $N2 - N4 > -0.5$.

We further divided the 25 sources into two sub-classes, in order to separate AGN candidates from normal star-forming galaxies. With Spitzer surveys, the IRAC colour-colour plot of $[3.6] - [5.8]$ vs $[4.5] - [8.0]$ has been proposed for use in selecting AGN candidates (Lacy et al., 2004). Similarly, Oyabu et al. (2007) show that X-ray detected AGNs are found to be systematically red in both $N2 - N4$ and $N3 - S7$ indicating power-law SEDs. Based on their

result, we adopt a colour cut of $N3 - S7 > -0.2$ for AGN candidates, which results in 11 AGN candidates in the $18\,\mu$m sample with $N2 - N3 > 0.1$. In Figure 3 (4) we show postage stamp images of 14 (11) $N2 - N3$-selected star-forming galaxies (AGN candidates) at R- and K_s-band and 9 IRC bands.

4.   SED fitting method

We analyse the SEDs of both 14 normal star-forming galaxies and 11 AGN candidates using the SED model of StarBUrsts with Radiative Transfer (SBURT; Takagi et al., 2003a, 2004). Since the contribution from AGN is not taken into account in SBURT, it is expected that the SEDs of AGN candidates show an excess in the MIR, owing to hot dust around the central massive black hole, while the best-fit model for normal star-forming galaxies would be largely acceptable.

We find the best-fit SED model from the prepared set of 540 SED models at various redshifts with different starburst age (0.01 – 0.6 Gyr), the compactness of the starburst region $0.3 \le \Theta \le 5.0$ and the extinction curve (MW, LMC and SMC type)[5]. The compactness of starbursts is defined by $r = \Theta (M_*/10^9 M_\odot)^{\frac{1}{2}}$ [kpc], where r and M_* are the radius and stellar mass of the starburst region, respectively. Note that the attenuation due to dust or A_V is a function of starburst age, peaking at $\sim t/t_0$ where t_0 is an evolutionary time-scale of starbursts taken to be 100 Myr. Also, the more compact the starburst region, i.e. smaller Θ, the larger the attenuation. The adopted SED models are the same as those used in Takagi et al. (2004) for the SED analysis of submm galaxies.

We searched for the best-fit SED model by χ^2-minimization. Considering the flux uncertainty with the IRC images and systematic errors between ground-based and space photometry, we set minimum flux errors at each photometric band, i.e. 5% for optical bands ($BVRi'z'$), 10% for J and K_s, 15% for $N2$ and $N3$, 30% for $N4$ and $S7$, and 20% for the other longer IRC bands. We have put larger minimum errors on $N4$ and $S7$ bands, since a systematic error on calibration is indicated from the SED of stars in our field (see also Lee et al. 2007). Since these minimum errors are chosen as the most conservative limit, the derived values of χ^2 can be regarded as the lower limits.

At rest frame UV wavelengths, the SEDs of starbursts could depend on the small scale geometry of gas/dust and stars resulting in the leakage of UV photons and affecting the resulting SED (c.f. Takagi et al., 2003a). Also note that the extinction curve is not well understood in starbursts in the UV. Therefore, considering these uncertainties in the SED model, we quadratically added an additional 20% error for data at rest-frame UV wavelengths, $<4000\,\text{Å}$, in order to reduce the statistical weight of data at the rest-frame UV. The adopted flux errors for the SED fitting are shown in Figure 5 and 6. We reject the SED

---

[5]   These SED models are available at http://www.ir.isas.jaxa.jp/~takagi/sedmodel/.

model if the value of χ^2 is significant at $< 1\%$ level.

5.   Results

5.1.   AGN/starburst diagnostics by the SED fitting

Figures 5 and 6 show the best-fit SBURT model for normal star-forming galaxies and AGN candidates respectively, including those rejected with a large χ^2 value (shown as dotted lines). As expected, most of the AGN candidates have power-law-like SEDs (see however ID25 as discussed below). According to the χ^2 values, SBURT has no acceptable best-fit model for 4 out of 14 star-forming galaxies, while 7 out of 11 AGN candidates cannot be explained by SBURT. For the majority of galaxies with no acceptable SED model, the large χ^2 is attributed to the excess of observed fluxes in more than 2 MIR bands, compared to the best-fit SED model. The detection of the MIR excess, probably due to the hot dust component around the central massive black hole, is reliable, thanks to the comprehensive wavelength coverage in the MIR. All the accepted models for AGN candidates (ID14, 35, 64, and 72) underestimate the MIR fluxes as well, but this does not much contribute to the χ^2 value, due to the large minimum error (30%) for $N4$ and $S7$. Thus, if more accurate photometry becomes possible for these bands, the rejection rate for AGN candidates could reach $\sim 100\%$. This result indicates that the simple colour selection of AGN candidates with AKARI bands is consistent with the more sophisticated diagnostics using the SED fitting.

Assuming all of the AGN candidates selected with $N2 - N3 > 0.1$ and $N3 - S7 > -0.2$ are indeed AGN, we estimate the AGN fraction of $18\,\mu$m-selected galaxies to be $15\pm4\%$ (11/72) in number or $\sim 12\%$ in total flux. Although the completeness correction is not yet applied, this fraction is consistent with previous MIR surveys (e.g. Fadda et al., 2002; Caputi et al., 2006). For example, Fadda et al. (2002) estimate that AGNs contribute $15\pm5\%$ of the total $15\,\mu$m flux in the Lockman Hole with a survey depth of $0.3\,$mJy at $15\,\mu$m. Manners et al. (2004) similarly find an AGN fraction of $\sim 19\%$ from Chandra follow up of $0.8 - 6\,$mJy $15\,\mu$m sources from the European Large Area ISO survey.

5.2.   Photometric redshift using MIR features

MIR photometry, such as Spitzer $24\,\mu$m band data, are rarely used to derive photometric redshifts (see however Pérez-González et al., 2005). By using the superb MIR coverage with the IRC photometry, it may be possible to constrain the redshifts of distant infrared galaxies by using the PAH and silicate absorption features. In Figure 5, we find that the steep rise in flux corresponding to the blue side of the $6.2\,\mu$m feature is successfully traced by the well-sampled IRC photometric bands; the best example of this can be seen in ID10. This is not possible with Spitzer photometry, which has a large gap between 8 and $24\,\mu$m. This new capability of the IRC may be useful for determining photometric redshifts for optically faint and featureless galaxies, such as young and dusty starburst galaxies with less prominent $4000\,\text{Å}$ breaks. However, it is

still necessary to calibrate the MIR photometric redshifts using spectroscopic follow-up observations.

In Figure 7, we show the comparison of photometric redshifts derived with *hyperz* using the ground-based optical-NIR photometry and those with the optical-to-IRC bands using SBURT. The majority of these photometric redshifts are consistent with one another within the 99% confidence limits. Significant discrepancies can be seen in ID14, 24, and 72. Among these, ID14 and 72 are AGN candidates, and ID24 is a star-forming galaxy. For AGN candidates, photometric redshifts from both *hyperz* and SBURT would not be reliable, since the adopted models do not include an AGN component. The star-forming galaxy ID24 has a nearly power-law-like SED in the optical-NIR bands, and therefore the photometric redshift using only the optical-NIR SED is likely to be unreliable. Photometric redshifts with the IRC bands could be most useful for this type of galaxy.

As suggested by Takagi & Pearson (2005), the PAH and silicate absorption features of galaxies at $z \sim 1$ could be identified using IRC 15, 18 and $24\,\mu$m photometry. Due to the relatively shallow depth of our $24\,\mu$m image, their 'silicate-break' selection technique is only partly applicable to our data. We discuss the application of this technique for our sample in section 6.

5.3. The nature of $18\,\mu$m-selected galaxies

Here we briefly describe the physical properties of the $18\,\mu$m-selected galaxies with $N2 - N3 > 0.1$ based on the results of the SED fitting using the SBURT model. More detailed analyses of AKARI MIR-selected galaxies will be given elsewhere.

The average 18μm flux of star-forming galaxies with $N3 - S7 < -0.2$ is $240\,\mu$Jy. In Table 2, we summarise the derived quantities from the SED fitting of the galaxies with acceptable χ^2 (i.e. not significant at $< 1\%$ level), along with the best-fit parameters. The average redshift of these galaxies is $\langle z \rangle = 1.0$. Infrared luminosities range from 10^{11} to $3 \times 10^{12} L_\odot$, and therefore they are classified as LIRGs or ULIRGs. From the SBURT model, a typical stellar mass of these (U)LIRGs is derived to be $3 \times 10^{10} M_\odot$, including galaxies as massive as $\sim 10^{11} M_\odot$.

It is interesting to note that no best-fit SED model shows prominent silicate absorption feature, i.e. they are less obscured objects, unlike nearby ULIRGs. There may be a systematic difference in the dust attenuation between low- and high-z objects with the same luminosity. At high redshifts, strong silicate absorption similar to nearby ULIRGs (e.g. Armus et al., 2007) is found in more luminous objects such as submm galaxies or MIR-selected galaxies with $> 10^{13} L_\odot$ (e.g. Houck et al., 2005). A systematic difference in the SEDs between ULIRGs at $z \lesssim 1$ and submm galaxies (i.e. Hy/ULIRGs at $z \sim 2$) is already reported as a systematic difference in dust temperatures (Chapman et al., 2005; Yang et al., 2007) and in the UV-submm SEDs (Takagi et al., 2004). Also, Reddy et al. (2006) claim that at a given bolometric luminosity the obscuration of galaxies is generally ~ 10 times smaller at $z \sim 2$ than at $z \sim 0$. The other possibility

is that our results indicate a selection effect, since ULIRGs with strong PAH emission should be brighter than obscured ULIRGs. A systematic difference in the SED of galaxies at different redshifts could be one of the most important topics for further work in the NEP survey.

Cases worthy of comment

ID10: The PAH emission of this galaxy is well sampled with the IRC photometry given the photometric redshift of $z_{\rm phot} = 0.6^{+0.1}_{-0.2}$. With MIR-L bands, the PAH $11.2\,\mu$m feature is covered. From the SED fitting, we find that the resulting χ^2 is 24.9 and half of this χ^2 value is explained by the $L15$ and $L18W$ bands alone, since the model overestimates the observed fluxes. This may indicate that the PAH emission of this galaxy has anomalous inter-band strength ratios. Certainly, we can put more strong constraints on this inter-band strength ratio once the spectroscopic redshift becomes available. With the mapping of the nearby spiral galaxy NGC6946 using AKARI/IRC at 7 and $11\,\mu$m and also the MIR spectroscopy, Sakon et al. (2007) report a strong variation of PAH $7.7/11.2\,\mu$m ratio, depending on the physical properties of interstellar medium. In the distant universe, galaxies with anomalous PAH inter-band ratio may exist in greater number than expected from the local universe.

ID25: Although this galaxy is classified as an AGN candidate, its SED is not characterized by a simple power-law. The $1.6\,\mu$m bump falls in between $N2$, $N3$ and $N4$ bands, suggesting that stellar emission dominates in this wavelength range. From $7\,\mu$m, there is a very steep rise in flux towards longer wavelengths which cannot be reproduced with the SBURT models.

ID26: This is an extremely red object with $R - K = 4.6$ (6.3 in Vega), and too red for the SBURT models within the reasonable parameter range for the SED fitting. Interestingly, the SED fitting with *hyperz* indicates that this is a young (40 Myr) and heavily obscured ($A_V = 5$) galaxy at $z = 1$. Also, this galaxy has the bluest $L15 - L18W$ colour in our sample, i.e. good candidate of silicate-break galaxy at $z \sim 1$ (see section 6).

ID65: This galaxy has a very steep power-law SED with the optical-to-IR slope of $\alpha \simeq -2.5$ when $f_\nu \propto \nu^\alpha$. This is very close to the maximum limit on the steepness for AGN SEDs (e.g. Alonso-Herrero et al., 2006).

6. Discussion

Takagi & Pearson (2005) proposed a new selection technique of high-z ULIRGs by using the AKARI/IRC multiwavelength survey, in which the colour anomaly in the MIR bands due to the silicate absorption feature is used. Galaxies found with this method are called silicate-break galaxies. Kasliwal et al. (2005) adopted this technique by using Spitzer $16\,\mu$m (IRS) and $24\,\mu$m (MIPS) observations. They found 36 candidate silicate-break galaxies probably at $1 \lesssim z \lesssim 1.8$ in $0.0392\,{\rm deg}^2$, corresponding ~ 920 sources deg^2.

Here we attempt to identify silicate-break galaxies with our data. As pointed out by Takagi & Pearson (2005),

the key wavelength for this selection method is $24\,\mu$m. Unfortunately, our 24μm image is not deep enough to employ the silicate-break technique. Instead, we use $L15$ and $L18W$.

In Figure 8, we show the colour-colour plot of $N2-N3$ vs. $L15-L18W$. According to Takagi & Pearson (2005), we could select ULIRGs at $z \sim 1$ with $L15-L18W \lesssim 0$, but we would suffer from the contamination from normal spiral galaxies at low redshifts. We use a colour cut of $N2-N3 > 0.1$ again to exclude the contamination from low-z galaxies.

We find that seven $18\,\mu$m-selected galaxies satisfy $N2-N3 > 0.1$ and $L15-L18W < 0$. Five out of seven, ID15, 16, 26, 58 and 60, have $N3-S7 < -0.2$, and are likely to be star-forming galaxies. Except for ID16 and 58, photometric redshifts (from both SBURT and *hyperz*) are consistent with the redshift expected from the silicate-break selection, i.e. $z \sim 1$. ID16 and 58 have $z_{\mathrm{phot}} = 0.6$ and 0.7, respectively. These low-z contaminants are expected, since the single colour cut $N2-N3 > 0.1$ is only useful for a rough selection of galaxies at $z \gtrsim 0.5$. Such contaminations would be reduced if we use a colour selection with 18 and $24\,\mu$m as suggested by Takagi & Pearson (2005).

As noted in section 5.3, no best-fit SED models for silicate-break galaxies have strong silicate absorption. So, they are not silicate-break but 'PAH'-break galaxies. On the other hand, Takagi & Pearson (2005) show that the SED of a silicate-break galaxy selected with the Spitzer IRS peak-up imager can be reproduced by an SED model with a strong silicate absorption feature. This galaxy is a submm galaxy and therefore more luminous than our $18\,\mu$m-selected galaxies. With deeper and wider MIR-L observations, we would find ULIRGs at $z \sim 1$ with silicate absorption, i.e. true silicate-break galaxies. More studies on the nature of silicate-break galaxies will be given elsewhere using the main NEP survey.

7. Summary

We investigated AKARI $18\,\mu$m-selected sources by using all nine IRC photometric bands, as a pilot study for the main AKARI NEP survey. By using the IRC observations for the monitor field, we detected 72 $18\,\mu$m sources from the area of 50.2 arcmin^2. In order to select galaxies at $z \gtrsim 0.5$, i.e. the main targets for the NEP survey, we employed a simple colour selection, $N2 - N3 > 0.1$ and obtained a sub-sample of 25. AGN candidates in this sub-sample are identified with another colour cut, $N3 - S7 > -0.2$, which implies a hot dust component. The resulting sample has 14 star-forming galaxies at $z \gtrsim 0.5$ and 11 AGN candidates with power-law like SEDs.

We analysed both star-forming galaxies and AGN candidates with a radiative transfer SED model of starbursts, SBURT (Takagi et al., 2003a). Since the SBURT model does not include an AGN component, the presence of an AGN can be assessed by the excess of observed flux at the MIR wavelengths due to hot dust around the central massive black hole. We found that our AGN candidates show MIR excesses compared to the best-fit SED models, most

of which are rejected at the significance of $< 1\%$ by the resulting large χ^2 value. This means that the simple colour selection for AGN candidates is consistent with the more sophisticated diagnostics with the SED model. An interesting future project would be SED analysis with more complicated models having both starbursts and AGN.

With the SED fitting, we obtained photometric redshifts using optical-to-MIR SEDs, which are largely consistent with ground-based optical-NIR photometric redshifts. We demonstrated that the steep rises in flux corresponding to the blue-side of the PAH $6.2\,\mu$m feature and also the flux dip between the PAH 7.7 and $11.2\,\mu$m features are recognizable in the resulting SEDs by IRC. The IRC all-band photometry is probed to be useful to constrain the redshift of infrared galaxies using the MIR spectral features.

Typically, $N2 - N3$-selected $18\,\mu$m sources are (U)LIRGs at $z \sim 1$ with masses $\sim 3 \times 10^{10} M_{\odot}$. No ULIRG in our sample has strong silicate absorption according to the best-fit SED model. This may suggest a systematic difference in the nature of ULIRGs at low and high redshifts, or may be a simple selection effect, owing to the faintness of ULIRGs with strong silicate absorption. We could test these hypotheses with deeper IRC all-band surveys such as the NEP-Deep survey.

This pilot study demonstrates well the interesting new capabilities of the AKARI NEP survey, compared to the existing infrared surveys by Spitzer. The IRC all-band photometry would be a powerful and unique tool to constrain the redshifts of optically faint heavily obscured galaxies. We may find many candidate examples of infrared galaxies with anomalous PAH inter-band strength ratio. Furthermore, unique samples of ULIRGs at $z \sim 1$ will be constructed with the silicate-break selection technique. Such samples could play an important role in revealing the nature of high-z ULIRGs, which should provide vital clues on the process of galaxy formation.

References

Alonso-Herrero, A., Pérez-González, P. G., Alexander, D. M., Rieke, G. H., Rigopoulou, D., Le Floc'h, E., Barmby, P., Papovich, C., Rigby, J. R., Bauer, F. E., Brandt, W. N., Egami, E., Willner, S. P., Dole, H., & Huang, J.-S. 2006, ApJ, 640, 167

Armus, L., Charmandaris, V., Bernard-Salas, J., Spoon, H. W. W., Marshall, J. A., Higdon, S. J. U., Desai, V., Teplitz, H. I., Hao, L., Devost, D., Brandl, B. R., Wu, Y., Sloan, G. C., Soifer, B. T., Houck, J. R., & Herter, T. L. 2007, ApJ, 656, 148

Babbedge, T. S. R., Rowan-Robinson, M., Vaccari, M., Surace, J. A., Lonsdale, C. J., Clements, D. L., Fang, F., Farrah, D., Franceschini, A., Gonzalez-Solares, E., Hatziminaoglou, E., Lacey, C. G., Oliver, S., Onyett, N., Pérez-Fournon, I., Polletta, M., Pozzi, F., Rodighiero, G., Shupe, D. L., Siana, B., & Smith, H. E. 2006, MNRAS, 370, 1159

Bertin, E. & Arnouts, S. 1996, A&AS, 117, 393

Bolzonella, M., Miralles, J.-M., & Pelló, R. 2000, A&A, 363, 476

Bruzual, G. & Charlot, S. 2003, MNRAS, 344, 1000

Caputi, K. I., Dole, H., Lagache, G., McLure, R. J., Puget, J.-L., Rieke, G. H., Dunlop, J. S., Le Floc'h, E., Papovich, C., & Pérez-González, P. G. 2006, ApJ, 637, 727

Caputi, K. I., Lagache, G., Yan, L., Dole, H., Bavouzet, N., Le Floc'h, E., Choi, P. I., Helou, G., & Reddy, N. 2007, ArXiv Astrophysics e-prints

Chapman, S. C., Blain, A. W., Smail, I., & Ivison, R. J. 2005, ApJ, 622, 772

Chary, R., Casertano, S., Dickinson, M. E., Ferguson, H. C., Eisenhardt, P. R. M., Elbaz, D., Grogin, N. A., Moustakas, L. A., Reach, W. T., & Yan, H. 2004, ApJS, 154, 80

Chary, R. & Elbaz, D. 2001, ApJ, 556, 562

Fadda, D., Flores, H., Hasinger, G., Franceschini, A., Altieri, B., Cesarsky, C. J., Elbaz, D., & Ferrando, P. 2002, A&A, 383, 838

Franceschini, A., Aussel, H., Cesarsky, C. J., Elbaz, D., & Fadda, D. 2001, A&A, 378, 1

Franceschini, A., Vaccari, M., Berta, S., Rodighiero, G., & Lonsdale, C. 2006, ArXiv Astrophysics e-prints

Genzel, R. & Cesarsky, C. J. 2000, ARA&A, 38, 761

Houck, J. R., Soifer, B. T., Weedman, D., Higdon, S. J. U., Higdon, J. L., Herter, T., Brown, M. J. I., Dey, A., Jannuzi, B. T., Le Floc'h, E., Rieke, M., Armus, L., Charmandaris, V., Brandl, B. R., & Teplitz, H. I. 2005, ApJL, 622, L105

Huang, J ., Rigopoulou, D., Papovich, C., Ashby, M. L. N., Willner, S. P., Ivison, R., Laird, E. S., Webb, T., Wilson, G., Barmby, P., Chapman, S., Conselice, C., Mcleod, B., Shu, C. G., Smith, H. A., Le Floc'h, E., Egami, E., Willmer, C. A. N., & Fazio, G. 2006, ArXiv Astrophysics e-prints

Huang, J.-S., Barmby, P., Fazio, G. G., Willner, S. P., Wilson, G., Rigopoulou, D., Alonso-Herrero, A., Dole, H., Egami, E., Le Floc'h, E., Papovich, C., Pérez-González, P. G., Rigby, J., Engelbracht, C. W., Gordon, K., Hines, D., Rieke, M., Rieke, G. H., Meisenheimer, K., & Miyazaki, S. 2004, ApJS, 154, 44

Imai, K., Matsuhara, H., Oyabu, S., Wada, T., Takagi, T., Fujishiro, N., Hanami, H., & Pearson, C. P. 2007, ArXiv Astrophysics e-prints

Kasliwal, M. M., Charmandaris, V., Weedman, D., Houck, J. R., Le Floc'h, E., Higdon, S. J. U., Armus, L., & Teplitz, H. I. 2005, ApJL, 634, L1

Kessler, M. F., Steinz, J. A., Anderegg, M. E., Clavel, J., Drechsel, G., Estaria, P., Faelker, J., Riedinger, J. R., Robson, A., Taylor, B. G., & Ximenez de Ferran, S. 1996, A&A, 315, L27

Lacy, M., Storrie-Lombardi, L. J., Sajina, A., Appleton, P. N., Armus, L., Chapman, S. C., Choi, P. I., Fadda, D., Fang, F., Frayer, D. T., Heinrichsen, I., Helou, G., Im, M., Marleau, F. R., Masci, F., Shupe, D. L., Soifer, B. T., Surace, J., Teplitz, H. I., Wilson, G., & Yan, L. 2004, ApJS, 154, 166

Lagache, G., Dole, H., Puget, J.-L., Pérez-González, P. G., Le Floc'h, E., Rieke, G. H., Papovich, C., Egami, E., Alonso-Herrero, A., Engelbracht, C. W., Gordon, K. D., Misselt, K. A., & Morrison, J. E. 2004, ApJS, 154, 112

Lee, H., Im, M., Wada, T., H., S., & et al. 2007, PASJ, this volume

Lutz, D., Valiante, E., Sturm, E., Genzel, R., Tacconi, L. J., Lehnert, M. D., Sternberg, A., & Baker, A. J. 2005, ApJL, 625, L83

Manners, J. C., Serjeant, S., Bottinelli, S., Vaccari, M., Franceschini, A., Perez-Fournon, I., Gonzalez-Solares, E., Willott, C. J., Johnson, O., Almaini, O., Rowan-Robinson, M., & Oliver, S. 2004, MNRAS, 355, 97

Matsuhara, H., Wada, T., Matsuura, S., Nakagawa, T., Kawada, M., Ohyama, Y., Pearson, C. P., Oyabu, S., Takagi, T., Serjeant, S., White, G. J., Hanami, H., Watarai, H., Takeuchi, T. T., Kodama, T., Arimoto, N., Okamura, S., Lee, H. M., Pak, S., Im, M. S., Lee, M. G., Kim, W., Jeong, W.-S., Imai, K., Fujishiro, N., Shirahata, M., Suzuki, T., Ihara, C., & Sakon, I. 2006, PASJ, 58, 673

Matsuhara, H., Wada, T., Pearson, C., Oyabu, S., & et al. 2007, PASJ, this volume

Menéndez-Delmestre, K., Blain, A. W., Alexander, D. M., Smail, I., Armus, L., Chapman, S. C., Frayer, D. T., Ivison, R. J., & Teplitz, H. I. 2007, ApJL, 655, L65

Murakami, H., Onaka, T., Nakagawa, T., Shibai, Y., & et al. 2007, PASJ, this volume

Neugebauer, G., Habing, H. J., van Duinen, R., Aumann, H. H., Baud, B., Beichman, C. A., Beintema, D. A., Boggess, N., Clegg, P. E., de Jong, T., Emerson, J. P., Gautier, T. N., Gillett, F. C., Harris, S., Hauser, M. G., Houck, J. R., Jennings, R. E., Low, F. J., Marsden, P. L., Miley, G., Olnon, F. M., Pottasch, S. R., Raimond, E., Rowan-Robinson, M., Soifer, B. T., Walker, R. G., Wesselius, P. R., & Young, E. 1984, ApJL, 278, L1

Onaka, T., Matsuhara, H., Wada, T., N., F., & et al. 2007, PASJ, this volume

Oyabu, S., Wada, T., Matsuhara, H., Pearson, C., & et al. 2007, PASJ, this volume

Pearson, C. 2005, MNRAS, 358, 1417

Pearson, C. P. 2001, MNRAS, 325, 1511

Pérez-González, P. G., Rieke, G. H., Egami, E., Alonso-Herrero, A., Dole, H., Papovich, C., Blaylock, M., Jones, J., Rieke, M., Rigby, J., Barmby, P., Fazio, G. G., Huang, J., & Martin, C. 2005, ApJ, 630, 82

Pope, A., Chary, R.-R., Dickinson, M., & Scott, D. 2006, ArXiv Astrophysics e-prints

Reddy, N. A., Steidel, C. C., Fadda, D., Yan, L., Pettini, M., Shapley, A. E., Erb, D. K., & Adelberger, K. L. 2006, ApJ, 644, 792

Sakon, I., Onaka, T., Wada, T., Ohyama, Y., & et al. 2007, PASJ, this volume

Takagi, T., Arimoto, N., & Hanami, H. 2003a, MNRAS, 340, 813

Takagi, T., Hanami, H., & Arimoto, N. 2004, MNRAS, 355, 424

Takagi, T. & Pearson, C. P. 2005, MNRAS, 357, 165

Takagi, T., Vansevicius, V., & Arimoto, N. 2003b, PASJ, 55, 385

Teplitz, H. I., Desai, V., Armus, L., Chary, R., Marshall, J. A., Colbert, J. W., Frayer, D. T., Pope, A., Blain, A., Spoon, H., Charmandaris, V., & Scott, D. 2007, ArXiv Astrophysics e-prints

Wada, T., Matsuhara, H., Oyabu, S., Onaka, T., & et al. 2007, PASJ, this volume

Weedman, D. W., Soifer, B. T., Hao, L., Higdon, J. L., Higdon, S. J. U., Houck, J. R., Le Floc'h, E., Brown, M. J. I., Dey, A., Jannuzi, B. T., Rieke, M., Desai, V., Bian, C., Thompson, D., Armus, L., Teplitz, H., Eisenhardt, P., & Willner, S. P. 2006, ApJ, 651, 101

Werner, M. W., Roellig, T. L., Low, F. J., Rieke, G. H., Rieke, M., Hoffmann, W. F., Young, E., Houck, J. R., Brandl, B., Fazio, G. G., Hora, J. L., Gehrz, R. D., Helou, G., Soifer, B. T., Stauffer, J., Keene, J., Eisenhardt, P., Gallagher, D., Gautier, T. N., Irace, W., Lawrence, C. R., Simmons, L., Van Cleve, J. E., Jura, M., Wright, E. L., & Cruikshank, D. P. 2004, ApJS, 154, 1

Xu, C. 2000, ApJ, 541, 134

Yan, L., Chary, R., Armus, L., Teplitz, H., Helou, G., Frayer, D., Fadda, D., Surace, J., & Choi, P. 2005, ApJ, 628, 604

Yang, M., Greve, T. R., Dowell, C. D., & Borys, C. 2007, ArXiv Astrophysics e-prints

Table 1. Summary of observations

Band	$\lambda_{\rm ref}^{a)}$ [μm]	Integration time [sec]	# of frames
N2	2.4	2112.1	51
N3	3.2	2029.3	49
N4	4.1	1490.9	36
S7	7.0	2503.6	153
S9W	9.0	2339.9	143
S11	11.0	1767.2	108
L15	15.0	736.3	45
L18W	18.0	763.3	45
L24	24.0	589.1	36

$^{a)}$ Reference wavelength

Table 2. Results of the SED fitting with SBURT$^{a)}$

ID	red. $\chi^{2\,b)}$	$z_{\rm phot}^{c)}$	Age [Gyr]	Θ	Ext.$^{d)}$	$\log L_{\rm IR}^{e)}$ [$L_\odot$]	$\log M_*$ [$M_\odot$]	$\log {\rm SFR}^{f)}$ [$M_\odot\,{\rm yr}^{-1}$]
6	2.14	$1.3^{+0.5}_{-0.2}$	0.5	1.2	LMC	12.0	11.0	2.0
10	2.07	$0.6^{+0.1}_{-0.2}$	0.4	1.6	MW	11.4	10.2	1.5
14$^{g)}$	1.39	$2.0^{+0.3}_{-0.7}$	0.3	2.0	LMC	12.5	11.1	2.6
15	1.16	$1.1^{+0.2}_{-0.3}$	0.4	2.0	MW	11.7	10.5	1.8
16	1.40	$0.5^{+0.2}_{-0.1}$	0.4	1.4	LMC	11.1	9.86	1.1
24	1.59	$1.0^{+0.2}_{-0.1}$	0.3	1.4	SMC	12.1	10.6	2.1
35$^{g)}$	1.16	$0.6^{+0.1}_{-0.2}$	0.6	1.2	MW	11.1	10.2	1.1
39	1.37	$1.1^{+0.4}_{-0.2}$	0.4	1.6	MW	11.7	10.4	1.7
52	1.41	$1.1^{+0.2}_{-0.2}$	0.2	2.0	LMC	12.0	10.2	2.1
58	1.48	$0.7^{+0.1}_{-0.2}$	0.4	1.4	LMC	11.4	10.1	1.4
60	0.71	$1.3^{+0.2}_{-0.3}$	0.2	2.0	SMC	12.2	10.4	2.3
64$^{g)}$	0.99	$1.1^{+0.9}_{-0.3}$	0.1	1.6	SMC	11.9	9.82	2.0
68	1.56	$0.9^{+0.3}_{-0.2}$	0.3	2.2	MW	11.5	10.1	1.6
70	1.14	$1.1^{+0.6}_{-0.4}$	0.3	2.4	MW	11.6	10.1	1.7
72$^{g)}$	2.15	$0.9^{+0.2}_{-0.2}$	0.1	1.0	SMC	12.0	9.83	2.1

$^{a)}$Rejected fitting results are not tabulated.

$^{b)}$Reduced χ^2

$^{c)}$Photometric redshifts with errors given at the 99% level

$^{d)}$Extinction curve

$^{e)}$Infrared luminosity with the wavelength range of $\lambda = 8 - 1000\,\mu$m
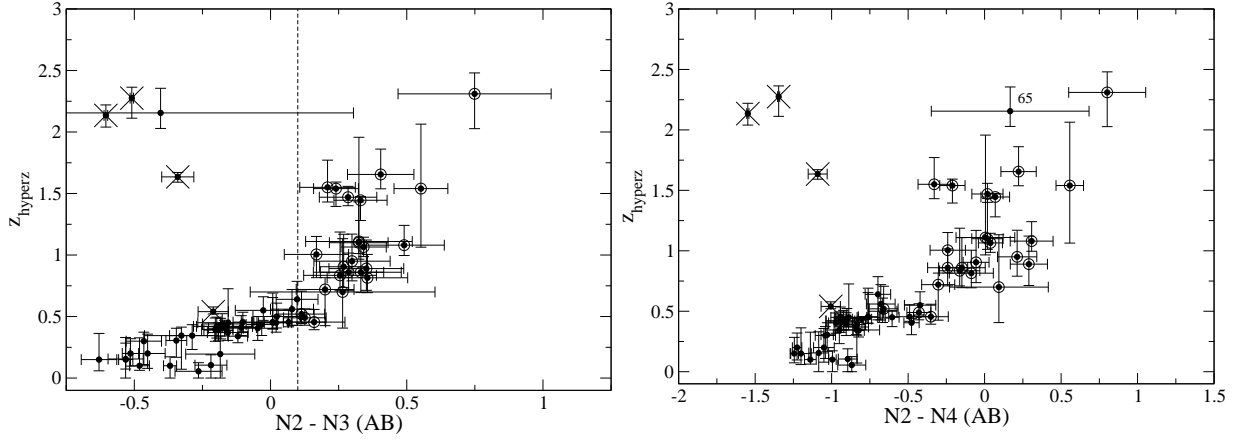
$^{f)}$Star formation rate

$^{g)}$AGN candidates

Fig. 1. Photometric redshifts derived from the ground-based optical-NIR SED by using *hyperz* as a function of the IRC NIR colour, $N2-N3$ and $N2-N4$. Errors of z_{hyperz} is the 99% confidence limit. Encircled dots are for galaxies with $N2-N3 > 0.1$. Most of the galaxies with $N2-N3 > 0.1$ can be selected with $N2-N4 > -0.5$. Large crosses indicate that the best-fit SED model is rejected with the significance of $< 1\%$. The tight correlation between photometric redshifts and NIR colours shows that a NIR colour cut can closely mimic a cut with the photometric redshift.
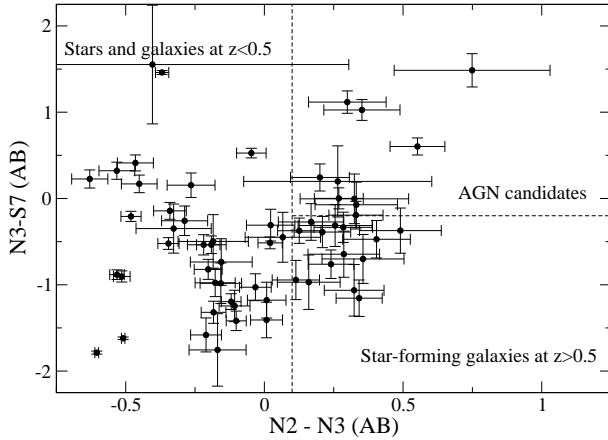
Fig. 2. $N2-N3$ vs. $N3-S7$ colour-colour diagram to classify $18\,\mu$m-selected galaxies into low-z ($z < 0.5$) galaxies, high-z star–forming galaxies and AGN candidates.
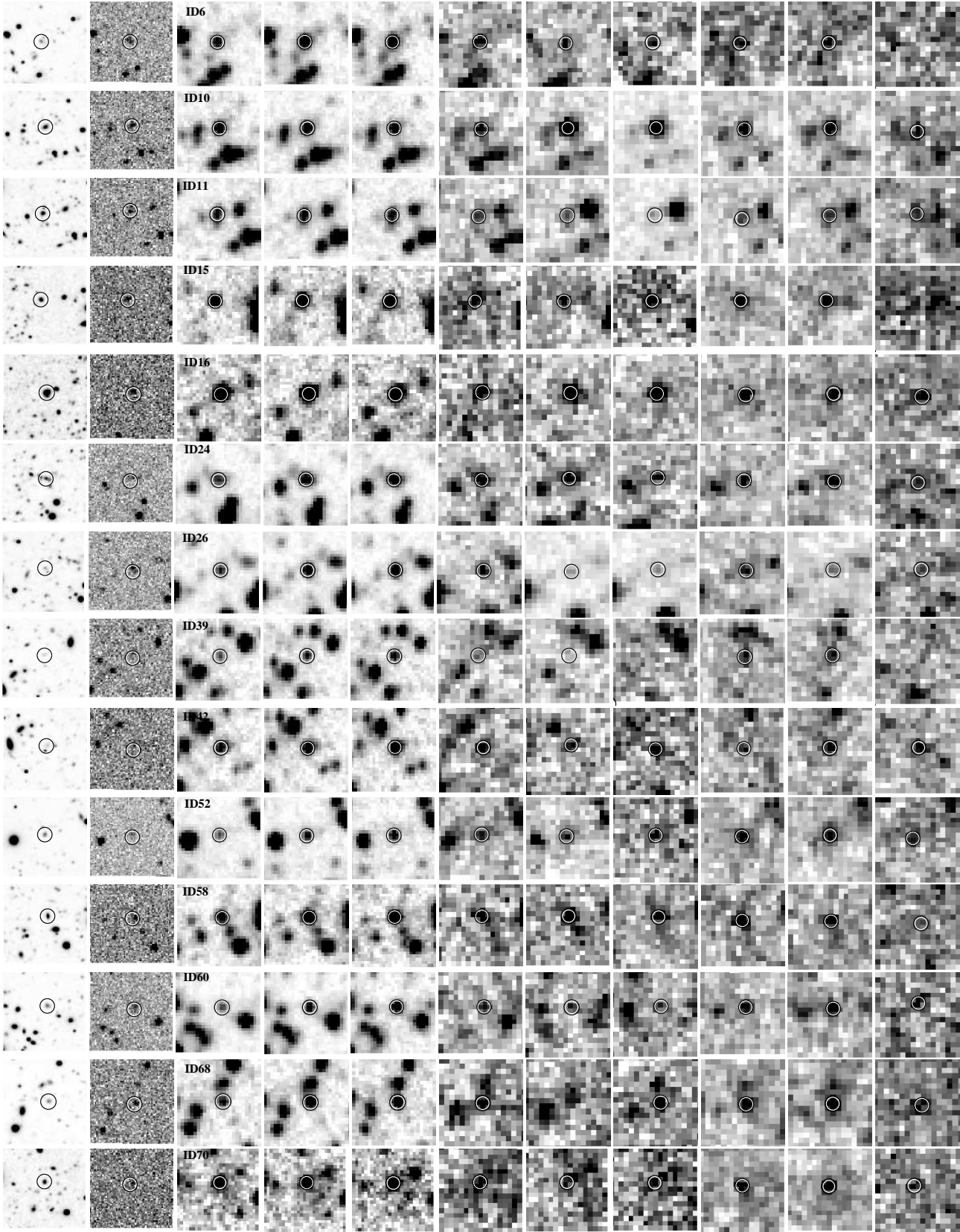
Fig. 3. Postage stamp image of $18\,\mu$m-selected galaxies with $N2 - N3 > 0.1$ and $N3 - S7 < -0.2$, i.e. star-forming galaxies at $z \gtrsim 0.5$. From left to right, we show R, K_s, $N2$, $N3$, $N4$, $S7$, $S9W$, $S11$, $L15$, $L18W$ and $L24$ band images. Identified $L18W$ sources are indicated with black and white circles with the radii of $3.5''$ and $3''$ respectively. The north is up and the east is to the left.
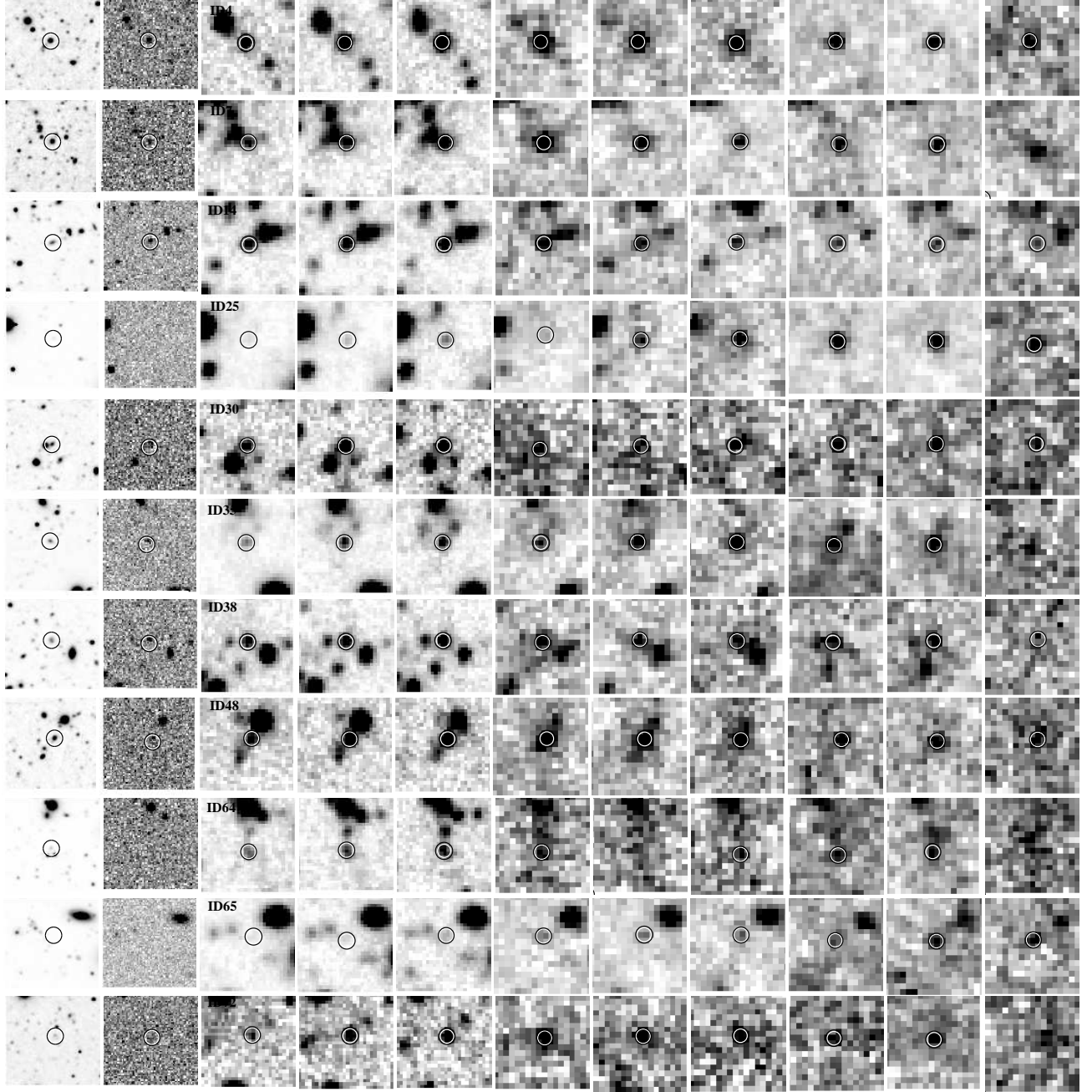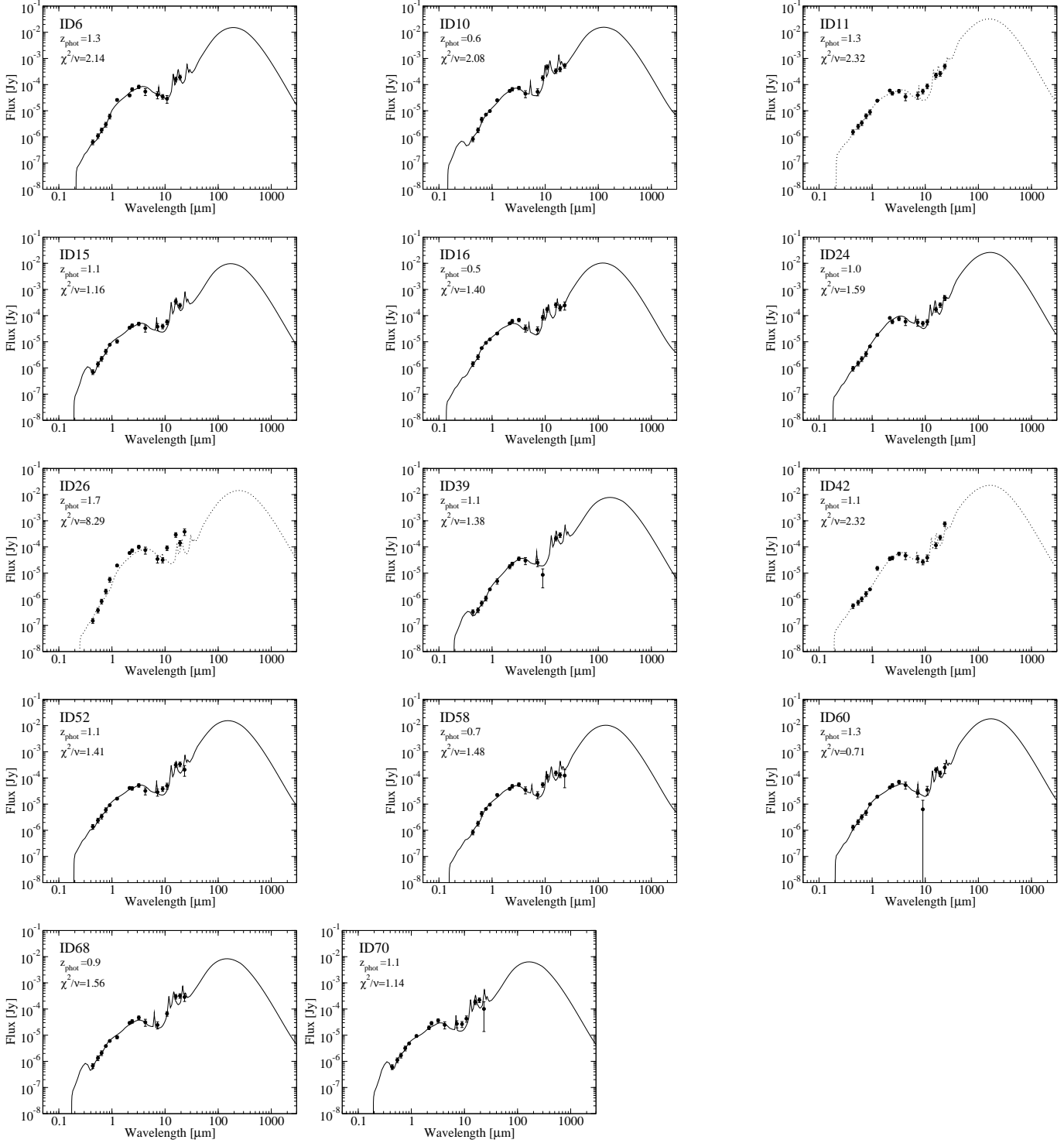
Fig. 4. Same as Figure 3, but for galaxies with $N2 - N3 > 0.1$ and $N3 - S7 > -0.2$, i.e. AGN candidates.

Fig. 5. Results of SED fitting for 18 μm-selected galaxies with $N2 - N3 > 0.1$ and $N3 - S7 < -0.2$, i.e. star-forming galaxies at $z \gtrsim 0.5$. The best-fit SED models rejected with the significance of $< 1\%$ are shown in dotted lines.
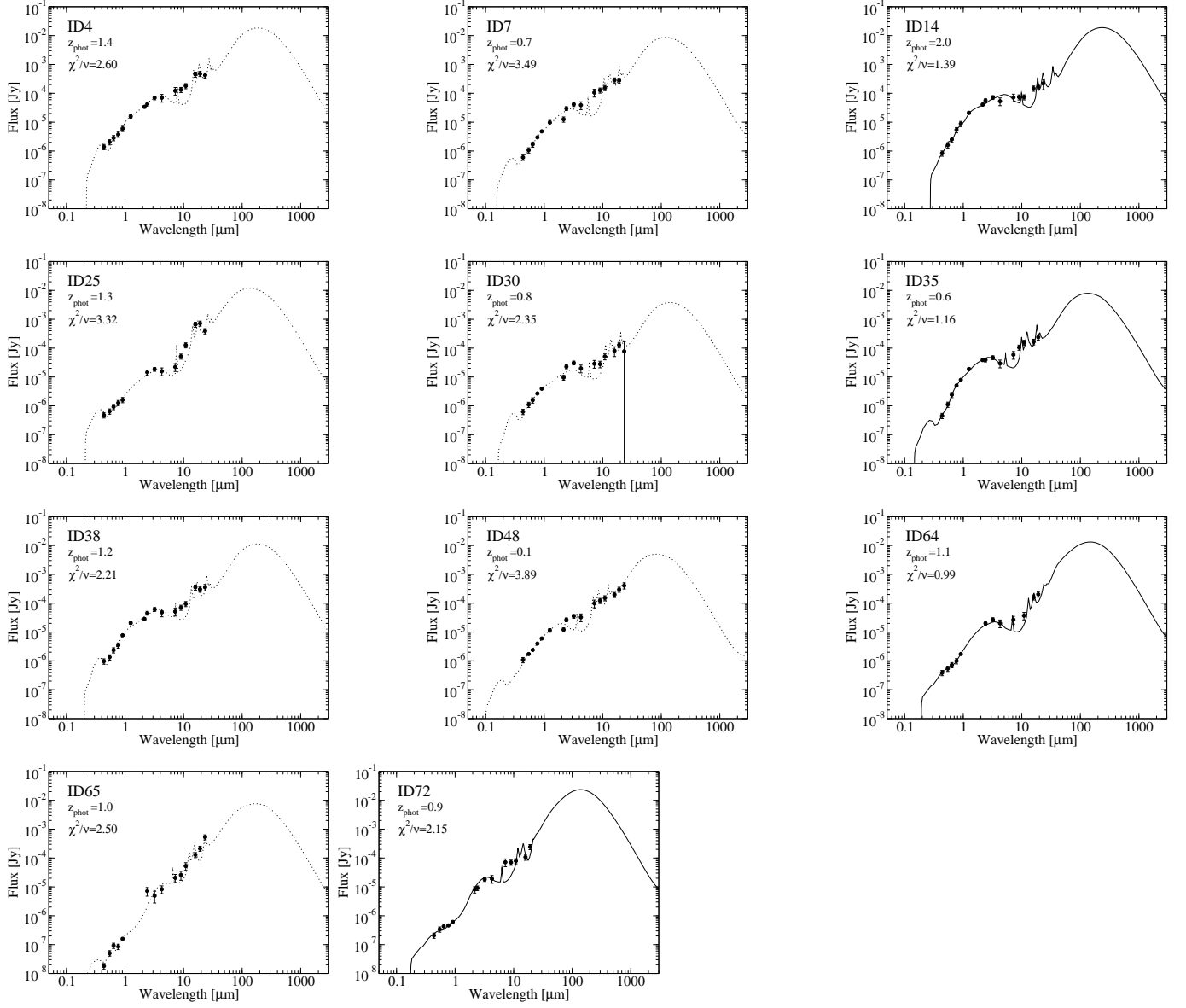
Fig. 6. Same as Figure 5, but for galaxies with $N2 - N3 > 0.1$ and $N3 - S7 > -0.2$, i.e. AGN candidates.
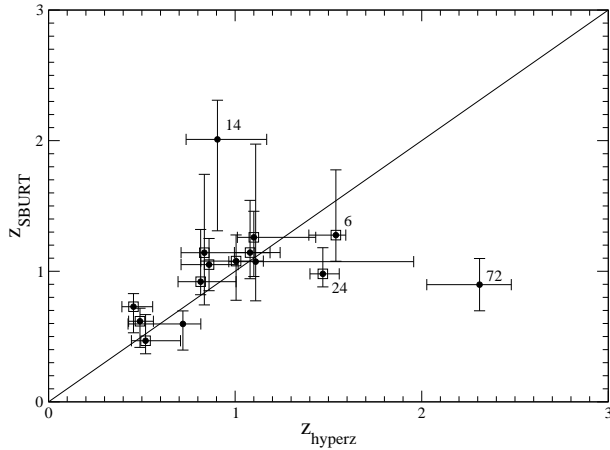

Fig. 7. Comparison of photometric redshifts derived from *hyperz* and SBURT. Errors on photometric redshifts are in 99% confidence limit. The numbers indicate the object ID of corresponding data points. Squares indicate star-forming galaxies.
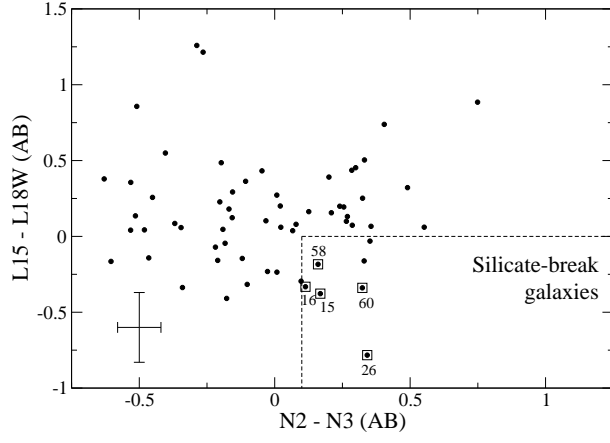
Fig. 8. Colour-colour plot to identify silicate-break galaxies. Squares indicate star-forming galaxies which satisfy selection criteria of silicate-break galaxies. The numbers indicate the object ID of corresponding data points.